Eur Biophys J (2009) 38:1115–1125
DOI 10.1007/s00249-009-0516-z

ORIGINAL PAPER

Fractal analysis and ionic dependence of endocytotic membrane activity of human breast cancer cells

Monika Krasowska · Zbigniew J. Grzywna · Maria E. Mycielska · Mustafa B. A. Djamgoz

Received: 13 March 2009 / Revised: 24 June 2009 / Accepted: 29 June 2009 / Published online: 18 July 2009

Abstract The endocytic membrane activities of two human breast cancer cell lines (MDA-MB-231 and MCF-7) of strong and weak metastatic potential, respectively, were studied in a comparative approach. Uptake of horseradish peroxidase was used to follow endocytosis. Dependence on ionic conditions and voltage-gated sodium channel (VGSC) activity were characterized. Fractal methods were used to analyze quantitative differences in vesicular patterning. Digital quantification showed that MDA-MB-231 cells took up more tracer (i.e., were more endocytic) than MCF-7 cells. For the former, uptake was totally dependent on extracellular Na^+ and partially dependent on extracellular and intracellular Ca^{2+} and protein kinase activity. Analyzing the generalized fractal dimension (D_q) and its Legendre transform $f(\alpha)$ revealed that under control conditions, all multifractal parameters determined had values greater for MDA-MB-231 compared with MCF-7 cells, consistent with endocytic/vesicular activity being more developed in the strongly metastatic cells. All fractal parameters studied were sensitive to the VGSC blocker tetrodotoxin (TTX). Some of the parameters had a "simple" dependence on VGSC activity, if present, whereby pretreatment with TTX reduced the values for the MDA-MB-231 cells and eliminated the differences between the two cell lines. For other parameters, however, there was a "complex" dependence on VGSC activity. The possible physical/physiological meaning of the mathematical parameters studied and the nature of involvement of VGSC activity in control of endocytosis/secretion are discussed.

Keywords Metastasis · Endocytosis · Voltage-gated Na^+ channel · Tetrodotoxin · Fractal

M. Krasowska · M. E. Mycielska · M. B. A. Djamgoz
Division of Cell and Molecular Biology, Neuroscience Solutions to Cancer Research Group, Imperial College London, Sir Alexander Fleming Building, South Kensington Campus, London SW7 2AZ, UK

M. Krasowska (✉) · Z. J. Grzywna
Section of Physics and Applied Mathematics, Department of Physical Chemistry and Polymer Technology, Silesian University of Technology, Strzody 9, 44-100 Gliwice, Poland
e-mail: Monika.Krasowska@polsl.pl

Introduction

An important issue in many fields of biophysics, medicine, and material sciences is the quantitative analysis of texture and patterns of objects and interpretation of structure–function relationships (Turiel 2003; Grzywna et al. 2003; Schroeder 1991; Krasowska et al. 2004a). Such patterns may often be complex and exhibit scale-dependent changes in structure. Some progress in this field has been made by means of studying the generalized fractal dimension, which can provide an effective quantitative description of the structure and morphology of a wide spectrum of different objects (Oiwa and Glazier 2004; Stosic and Stosic 2006). Indeed, fractal methods are also being used increasingly to analyze biological structures and cellular phenomena, including pathology, vascular architecture, tumor/parenchymal borders, and nuclear morphology (Cross and Cotton 1992; Losa 1995; Cross 1997; Coffey 1998; Baish and Rakesh 2000; Simeonov and Simeonova 2006; Stosic and Stosic 2006). Although tumor biology is extremely complex, application of integrative mathematical techniques promises to formalize some of the underlying basic mechanisms and, ultimately, provide a holistic understanding (Anderson and Quaranta 2008). In particular, fractal geometry has been suggested to be useful in

characterizing and diagnosing metastatic tumors (de Pillis et al. 2005). In a previous study, Krasowska et al. (2004) showed that multifractal methods can be used to analyze vesicular patterning resulting from endocytic membrane activity in rat prostate cancer (PCa) cells. This analysis revealed (1) that values of the fractal parameters were higher in strongly vs. weakly metastatic cells and (2) that pharmacological treatment changed the values in line with altered metastatic potential. It was concluded that fractal analysis could be used to analyze rat prostate cancer cells' metastatic status. However, it is not known if fractal analysis of vesicular activity might be applicable to other cancers.

Breast cancer (BCa) is the most common type of cancer and the second leading cause of death from cancer in women (Parkin et al. 1999). It is metastasis, the spreading of cancer, that is the major cause of mortality in BCa, as in most other cancers (Liotta 1986; Eccles et al. 2007). Several problems remain in the clinical management of BCa, especially as regards definitive diagnosis and long-lasting effective, nontoxic therapy (Ali and Coombes 2002). Endocytosis, vesicular retrieval, and internalization of plasma membrane are critical components of the basic cancer process (Polo et al. 2004). Endocytosis can relate to metastasis in at least two respects. First, it is a reflection of exocytosis, i.e., vesicular secretion, possibly of growth factors and cytokines that cancer cells may release (Wong et al. 2003; Hall et al. 2003). Second, endocytosis is a means of regulating functional protein expression in the plasma membrane, which is important to cellular signalling, as in the case of epidermal growth factor receptor activity (Rubin et al. 2003; Fong et al. 2003; Gundelfinger et al. 2003). Finally, endocytosis may also be associated with drug resistance (Liang et al. 2006).

Breast cancer cells with different pathological characteristics differ markedly in their ion channel expression. In particular, only strongly metastatic BCa (MDA-MB-231) cells express functional voltage-gated Na^+ channels (VGSCs) (Roger et al. 2003; Fraser et al. 2005). The latter commonly are involved in endocytic/secretory membrane activity in cells, including tumor cells (Murakami et al. 1998; Mycielska et al. 2003; Onganer and Djamgoz 2005). The main VGSC in metastatic BCa cells was found to be the neonatal splice variant of Nav1.5 (Fraser et al. 2005; Brackenbury et al. 2007). Such channels are blocked by micromolar concentrations of tetrodotoxin (TTX), in contrast to VGSC (Nav1.7) expression in PCa cells, which is sensitive to TTX in the nanomolar range (Brackenbury et al. 2007). Micromolar TTX, as well as small-interfering RNA and a polyclonal antibody for Nav1.5 suppressed a range of cellular behaviors that are involved in the metastatic cascade in BCa (Fraser et al. 2005; Brackenbury et al. 2007). Interestingly, the kinetics of ion channels themselves may follow fractal principles (Liebovitch and Toth 1990).

The main aim of the present study was to extend the fractal analysis approach to human BCa cells of markedly different metastatic potentials. A secondary aim was to investigate the ionic dependence of endocytosis.

Materials and methods

Cell culture

MDA-MB-231 and MCF-7 cell lines (strongly and weakly metastatic, respectively) were grown in DMEM supplemented with 4 mmol/l and 5–10% fetal bovine serum (Fraser et al. 2005).

Tracer (horseradish peroxidase) uptake and release

These experiments were carried out as described previously (Mycielska et al. 2003; Krasowska et al. 2004a; Fraser et al. 2005). Uptake of horseradish peroxidase (HRP; Sigma type VI) was performed in mammalian physiological saline (MPS) solution in which the cells were first carefully rinsed. In most experiments, cells were incubated with 0.5 mg/ml HRP for 40 min, reconfirmed as optimal, as determined previously (Fraser et al. 2005). Following fixing, dehydration, and cytochemistry analysis, the cells were mounted in DPX. Labelled cells were imaged under a Zeiss Axiovert microscope using a 100× oil immersion objective (Fig. 1). Typical images were digitized using a CoolSNAP camera, and measurements were made using Image-Pro Plus software (Media Cybernetics, MD, USA) (Fig. 1). In experiments aimed at measuring the release of vesicles (exocytosis), uptake was induced as above but cytochemistry analysis was performed after a time period of up to 2 h. The difference in the staining between the maximum (i.e., staining obtained immediately after the uptake) and at a specified time was assumed to represent release over that period.

Ionic substitutions and pharmacology

The control Ringer (MPS) solution had the following composition (in mM): NaCl (144), KCl (5.4), $MgCl_2$ (1), $CaCl_2$ (2.5), D-glucose (5.6), and HEPES (5), adjusted to pH 7.2. Essential details of the ionic substitutions are given in Table 1. In the Na^+-free solution, all NaCl was substituted with equimolar choline chloride. A high-K^+ solution was made by increasing the KCl concentration 10-fold, whilst reducing NaCl by the same amount. A control solution for the latter contained the control amount of K^+ (5.4 mM) with NaCl reduced to the same level as in the

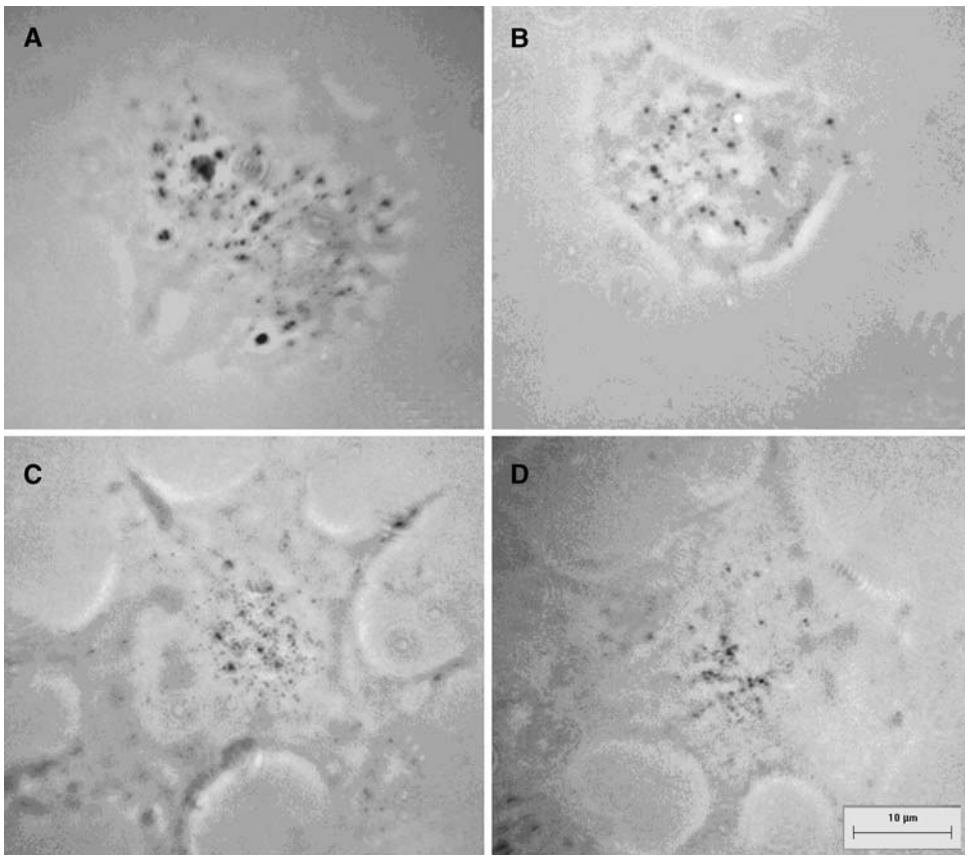

Fig. 1a–d Typical light micrographs of breast cancer cells. **a**, **b** MDA-MB-231 cells and **c**, **d** MCF-7 cells showing endocytic/vesicular uptake of HRP under different conditions. **a**, **c** Controls [uptake under normal tissue culture conditions (i.e., with no tetrodoxin present)]. **b**, **d** Cells pretreated with tetrodotoxin (1 µM). *Scale bar* applies to all parts of the figure. Generally, under control conditions, vesicles formed larger aggregates of "vacuoles" distributed throughout the cytoplasm in MDA-MB-231 cells. Staining in MCF-7 cells was "finer" and appeared more concentrated around the nucleus. After application of TTX, structures in both cell lines were similar

Table 1 Ionic compositions of solutions

Solution	NaCl (mM)	KC1 (mM)	$CaCl_2$ (mM)	$MgCl_2$ (mM)	D-glucose (mM)	HEPES (mM)	Choline CI (mM)	pH
Normal	144	5.4	2.5	1	5.6	5	–	7.2
Na^+-free	–	5.4	2.5	1	5.6	5	144	7.2
High-K^+	95.4	5.4	2.5	1	5.6	5	–	7.2
High-K^+ control	95.4	5.4	2.5	1	5.6	5	48.6	7.2
Ca^{2+}-free	144	5.4	–	1	5.6	7.5	–	7.2

high-K^+ solution, with choline chloride as the substitute. The following pharmacological agents (added directly to MPS) were used: TTX (0.01–10 µM), aconitine (400 µM), thapsigargin (1 µM), and KT5720 (50 nM).

Quantification of tracer uptake and release

The amount of endocytotic staining (E_n) relative to whole cell size was quantified as follows:

$$E_n(\%) = \left[A_{\text{hrp}}/A_{\text{total}}\right] \times 100 \quad (1)$$

where A_{hrp} is the HRP-stained area and A_{total} is the total cross-sectional area of the cell deduced from its outline (Mycielska et al. 2003). Release of HRP ("exocytosis"; E_x) was quantified as the value of E_n decreasing, as tracer was released following full uptake in a given experiment.

Fractal analyses

The patterns of staining were analyzed by multifractal analyses (Djamgoz et al. 2001; Grzywna et al. 2001; Krasowska et al. 2004a). We used a "box-counting method" (BCM) for evaluating multifractal spectra (Fig. 2). BCM is one of the most common methods for calculating fractal characteristics and generalized fractal dimensions of a self-similar object (e.g., Avnir 1989; Almqvist 1996; Bassingthwaight et al. 1994; Liebovitch 1998). By covering a structure with boxes of length ε, the generalized fractal dimension can be defined as follows:

$$D_q = \frac{1}{q-1}\lim_{\varepsilon \to 0}\frac{\ln \sum_{i=1}^{M(\varepsilon)} P_i^q}{\ln \varepsilon} \quad (2)$$

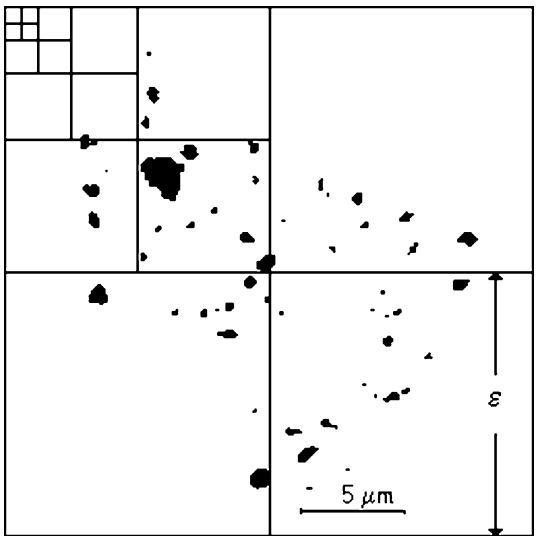

Fig. 2 The box covering/counting method used for the fractal analyses of cells. The image was covered with *boxes* of varying sizes (ε). As the box length is decreased, the new number of boxes is counted. The fractal dimension is obtained by plotting $N(\varepsilon)$ versus $1/\varepsilon$ in a double logarithmic plot. The curve is approximated by a linear regression, and the slope is determined as the box dimension. For D_q, we also used P_i as the probability of finding a point in the ith element of covering

where q is a real number (dimension index), P_i is the probability of finding a point in the ith element of covering, ε is the width of the covering element, and $M(\varepsilon)$ is the number of covering elements. The $f(\alpha)$ formalism ("multifractal spectrum"), a Legendre transform of D_q, is defined as follows:

$$f(\alpha) = \alpha\tilde{q}(\alpha) - \tau_{\tilde{q}(\alpha)} \quad (3)$$

where $\alpha = \frac{\partial \tau_q}{\partial q}$, and $\tau_q = (q-1)D_q = \lim_{\varepsilon \to 0} \frac{\ln \sum_{i=1}^{N(\varepsilon)} P_i^q}{\ln \varepsilon}$, and $\tilde{q}$ is the dimension index. The full derivation of this transform was given earlier in the paper by Krasowska et al. (2004a). $f(\alpha)$ is analogous to entropy with α (slope of straight line in the transform), corresponding to total energy (Stanley 1996). $D_{-\infty}$ and D_{∞} depend on extreme values of P_i, and their difference (Δ) describes the range of values of P_i. Thus, we used the ΔD ($D_{-\infty} - D_{\infty}$) as a new measure of self-similarity of stochastic fractals. For ideal/deterministic fractals, the value of ΔD equals 0. The great value of $D_{-\infty}$ indicates the existence of very rarefied regions. On the contrary, the not-so-small value of D_{∞} allows the conclusion that the more dense regions are not very concentrated. Further details of the BCM method and fractal analyses were published earlier (Grzywna et al. 2001; Grzywna et al. 2003, Krasowska et al. 2004a). The "partitioned iterated function system-semifractal" ($N_{PFIS\text{-}SF}S$), a deterministic algorithm decoding the image analysis, was used as described before (Grzywna and Stolarczyk 2002; Krasowska et al. 2004a).

Data handling

For each condition, at least three independent experiments were performed. The mean values of E_n, E_x, and D_q were determined for 30–50 cells from each dish. The value of each parameter was averaged for the 100–150 cells, and the standard error was calculated. Student's t-test was used for statistical analyses.

Results

Typical light micrographs of MDA-MB-231 and MCF-7 cells labelled by endocytic/vesicular uptake of HRP and a corresponding digital image are shown in Fig. 1. The quantitative data obtained are summarized in Table 2.

Basic observations: tracer uptake and release

The uptake of HRP was dose-dependent. Increasing the HRP concentration from 0.25 to 0.5 mg/ml (for fixed time of 40 min) led to increased uptake in both MDA-MB-231 cells ($E_n = 0.53 \pm 0.04$ and $1.91 \pm 0.16\%$) and MCF-7 cells ($E_n = 0.31 \pm 0.09$ and $0.81 \pm 0.05\%$). In each case, the increase was highly significant ($P < 0.005$). There was a further but smaller increase in uptake when the HRP concentration was raised to 1 mg/ml ($E_n = 2.10 \pm 0.16\%$ for MDA-MB-231 and $0.85 \pm 0.12\%$ for MCF-7 cells). At given concentrations tested, MDA-MB-231 cells were 135% more endocytic than MCF-7 cells ($P < 0.05$).

The uptake of HRP was also time-dependent (Fig. 3a). There was a rapid increase in uptake in the first 40 min of incubation: $E_n = 0.33 \pm 0.14\%$ (10 min) and $0.81 \pm 0.05\%$ (40 min) for MCF-7 cells; $E_n = 0.51 \pm 0.08\%$ (10 min) and $1.91 \pm 0.15\%$ (40 min) for MDA-MB-231 cells ($P < 0.01$ for all). Longer incubation of the cells with HRP, up to 2 h, led to much smaller, although still significant, increases in uptake ($E_n = 0.82 \pm 0.02\%$ for MCF-7 and $E_n = 1.93 \pm 0.14\%$ for MDA-MB-231, respectively; $P < 0.05$ in each case).

Following preloading of the cells in the normal way, HRP staining (E_x) declined as exocytosis occurred (Fig. 3b). In both cell lines, two phases of release were observed relative to their respective original preloaded control levels (Fig. 3b). First, there was a brisk 20-30% drop in staining during the first 10 min of washing. Then, the release became much smaller. In both phases, MDA-MB-231 cells were more exocytotic than MCF-7 cells.

The remainder of the experiments were carried out on endocytosis, and 0.5 mg/ml HRP over 40 min was used for optimal uptake.

Table 2 Summary of quantitative data (means ± standard errors) obtained from the different analytical approaches employed in the present study (digital imaging and analyses of multifractals)

	MDA-MB-231 (control)	MCF-7 (control)	MDA-MB-231 (TTX)	MCF-7 (TTX)
$D_{-\infty}$	3.62 ± 0.06	2.19 ± 0.04	2.99 ± 0.05	2.68 ± 0.05
D_{-10}	3.38 ± 0.06	2.06 ± 0.04	2.79 ± 0.05	2.52 ± 0.05
D_{-5}	3.10 ± 0.06	1.92 ± 0.04	2.56 ± 0.05	2.34 ± 0.05
D_{-4}	2.97 ± 0.06	1.86 ± 0.04	2.46 ± 0.05	2.26 ± 0.05
D_{-3}	2.80 ± 0.06	1.77 ± 0.04	2.31 ± 0.05	2.14 ± 0.05
D_{-2}	2.53 ± 0.06	1.65 ± 0.04	2.08 ± 0.05	1.95 ± 0.05
D_{-1}	2.14 ± 0.06	1.46 ± 0.04	1.71 ± 0.05	1.61 ± 0.05
D_0	1.71 ± 0.06	1.19 ± 0.04	1.23 ± 0.05	1.1 1 ± 0.05
D_1	1.40 ± 0.06	0.96 ± 0.04	0.96 ± 0.05	0.69 ± 0.05
D_2	1.23 ± 0.06	0.82 ± 0.04	0.83 ± 0.05	0.52 ± 0.05
D_3	1.15 ± 0.06	0.75 ± 0.04	0.77 ± 0.05	0.45 ± 0.05
D_4	1.10 ± 0.06	0.71 ± 0.04	0.73 ± 0.05	0.42 ± 0.05
D_5	1.07 ± 0.06	0.69 ± 0.04	0.70 ± 0.05	0.41 ± 0.05
D_{10}	1.00 ± 0.06	0.64 ± 0.04	0.66 ± 0.05	0.37 ± 0.05
$D_{+\infty}$	0.94 ± 0.06	0.59 ± 0.04	0.61 ± 0.05	0.34 ± 0.05
ΔD	2.69 ± 0.06	2.38 ± 0.04	1.60 ± 0.05	2.34 ± 0.05
$N_{PIFS\text{-}SF}S$	178 ± 49	62 ± 17	52 ± 9	51 ± 18

Parameters are defined in the text. Each data set was obtained from the measurement of 100–150 cells, from at least three different experiments

Effects of VGSC blocker and opener on tracer uptake

Incubation of MDA-MB-231 cells in HRP together with the VGSC blocker TTX (1 μM) resulted in a significant (51%) decrease in uptake ($E_n = 0.94 \pm 0.13$, $P < 0.01$). There was no difference in the endocytic activities of TTX-treated MDA-MB-231 cells and control (untreated) MCF-7 cells ($P > 0.05$). Co-treatment of MDA-MB-231 cells with HRP and aconitine (400 μM) resulted in a small but significant (18%) increase in uptake ($E_n = 2.25 \pm 0.18$; $P < 0.01$). In contrast, the same working concentrations of TTX and aconitine had no effect on HRP uptake in the MCF-7 cells ($E_n = 0.82 \pm 0.07$ and 0.79 ± 0.10, respectively).

Effects of ionic substitutions and modulators

Data on the effects of ionic substitutions and modulators are shown in Fig. 4. In the absence of Na^+, HRP uptake by MDA-MB-231 was significantly reduced ($E_n = 0.91 \pm 0.32$), whilst the same treatment had a much smaller effect on MCF-7 cells ($E_n = 0.74 \pm 0.03$). There was no difference in the values of E_n for MDA-MB-231 cells treated with TTX and Na^+-free MPS ($P > 0.05$).

Increasing the extracellular K^+ concentration 10-fold from 5.4 to 54 mM reduced HRP uptake in both cells: $E_n = 0.81 \pm 0.36$ (MDA-MB-231 cells) and 0.58 ± 0.09

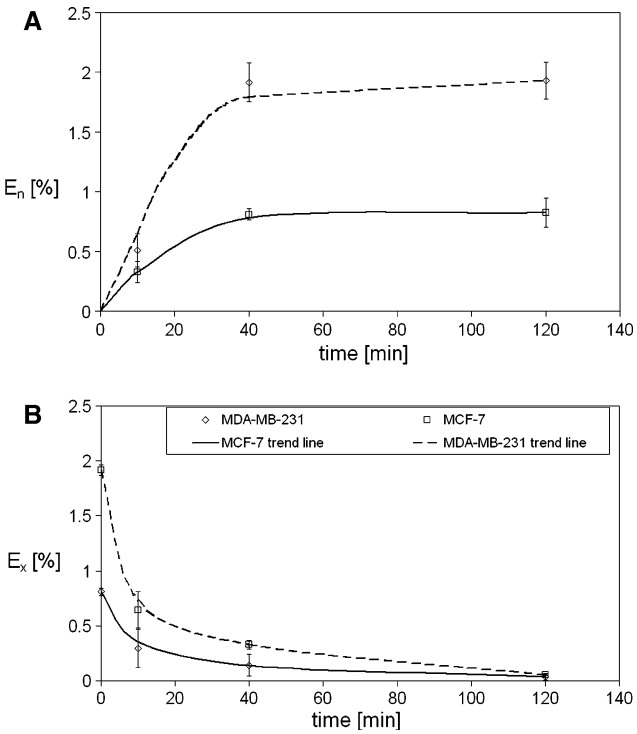

Fig. 3 Time dependence of HRP uptake into (**a**) and release from (**b**) MDA-MB-231 and MCF-7 cells. Uptake and release of HRP were quantified by the parameters E_n and E_x, respectively. Data points represent means ± standard errors

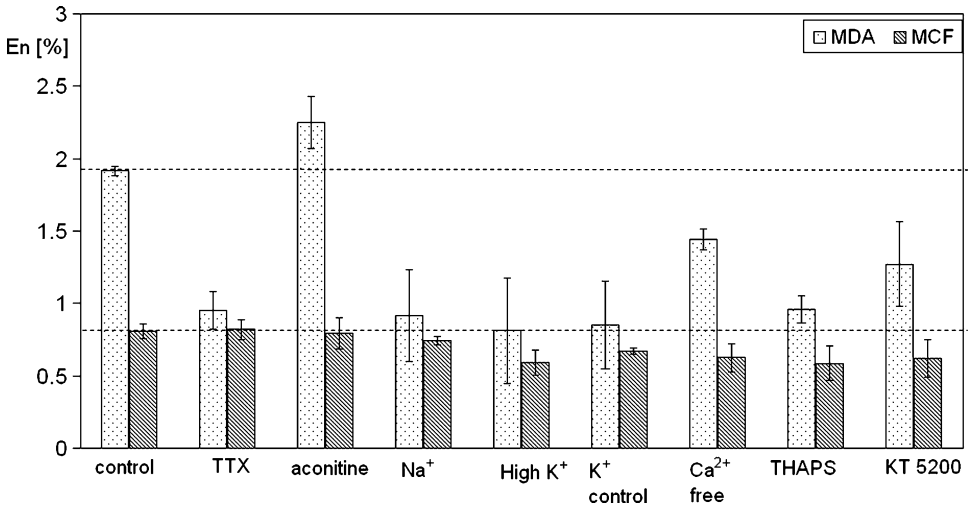

Fig. 4 Averaged (E_n) data (HRP uptake) for MDA-MB-231 and MCF-7 cells under various ionic conditions: control (MPS), TTX (1 μM), aconitine (400 μM), Na^+-free, high-K^+, high-K^+ control, Ca^{2+}-free, thapsigargin/THAPS (1 μM), and KT5200 (50 nM). *Columns* denote the mean ± standard error. The *dotted horizontal lines* indicate the control levels for the two cell lines, for comparison

(MCF-7 cells). These changes were significant ($P < 0.01$). Reducing the extracellular Na^+ concentration by 38.5 mM (as a control for the high-K^+ treatment) also reduced HRP uptake in both cell lines. In fact, there was no difference in the values of E_n for high-K^+ and K^+-control solutions. It was concluded that the effect of the high-K^+ solution, in fact, was due to the concomitant decrease in Na^+.

Uptake of HRP into MDA-MB-231 cells was partially dependent on Ca^{2+}. Thus, removal of extracellular Ca^{2+} resulted in a 24% decrease in HRP uptake ($E_n = 1.44 \pm 0.07$; $P < 0.05$). Possible involvement of intracellular Ca^{2+} stores was tested by incubating the cells with thapsigargin, an inhibitor of sarco/endoplasmic reticulum Ca^{2+} ATPase (SERCA). This resulted in a significant (50%) decrease in uptake of HRP by MDA-MB-231 cells ($E = 0.96 \pm 0.09$; $P < 0.01$). Neither treatment involving Ca^{2+} had an effect on MCF-7 cells ($E_n = 0.62 \pm 0.09$ and 0.58 ± 0.12, respectively; $P > 0.05$ for both).

In several cell types, Ca^{2+}-independent vesicular activity has previously been shown to be controlled by protein kinase A (PKA) (Seino and Shibasaki 2005). Finally, therefore, the possible role of PKA in endocytosis was investigated by treating the cells with KT5200, an inhibitor of PKA. This resulted in a significant (34%) decrease in MDA-MB-231 cells' HRP uptake ($E_n = 1.27 \pm 0.29$; $P < 0.01$ cf. control). Interestingly, with KT5200 there was also an effect on HRP uptake in the MCF-7 cells ($E = 0.62 \pm 0.13$; $P > 0.05$).

Fractal analyses

As can be seen on Fig. 1, the patterning of the labelled vesicles also differed significantly between the two cell lines. On the whole, vesicles formed larger aggregates of "vacuoles" distributed throughout the cytoplasm in MDA-MB-231 cells. On the other hand, staining in MCF-7 cells was "finer" and appeared more concentrated around the nucleus. Fractal analyses were performed on cells under control conditions and following treatment with VGSC modulators (i.e., TTX and aconitine). The results of these analyses are shown in Figs. 5 and 6 and summarized in Table 2. Figure 5 shows the generalized fractal dimensions (D_q) and the multifractal spectra [$f(\alpha)$] for control and TTX-treated MDA-MB-231 and MCF-7 cells. Clearly, there were notable differences between the parameters for the two cell lines, and TTX had a major effect on MDA-MB-231 cells (Figs. 5, 6 and Table 2).

The value of the fractal dimension D_0 was significantly bigger for MDA-MB-231 compared with MCF-7 cells (1.71 ± 0.05 vs. 1.19 ± 0.05; $P < 0.003$). Treatment with TTX induced a significant shift for MDA-MB-231 but not MCF-7 cells, $D_0 = 1.23 \pm 0.05$ and 1.11 ± 0.05, respectively. This shift was significant for MDA-MB-231 ($P < 0.01$) but not MCF-7 cells ($P > 0.05$). In fact, following the TTX treatment, the difference in the values of D_0 for the two cell lines disappeared ($P > 0.05$). The effects of removing Na^+ from the incubation medium were broadly the same as TTX (not shown). Incubation of MDA-MB-231 cells with aconitine resulted in a slight (7%) increase in the value of D_0 (to 1.76 ± 0.05), but this change was not significant ($P > 0.05$). Aconitine had hardly any effect on the D_0 value for MCF-7 cells (1.23 ± 0.05 vs. 1.19 ± 0.05, control).

The value of ΔD was higher for MDA-MB-231 compared with MCF-7 cells (2.69 ± 0.05 vs. 2.38 ± 0.05; $P < 0.01$). In the presence of TTX, there was a large decrease in the value of ΔD for MDA-MB-231 (to 1.60 ± 0.05; $P < 0.01$) but not for MCF-7 cells ($\Delta D = 2.34 \pm 0.05$; $P > 0.05$). Treatment with aconitine induced a slight (9%) increase in the value of ΔD for MDA-MB-231 cells (to 2.93 ± 0.05) but this was not significant ($P > 0.05$). In the case of MCF-7 cells, aconitine decreased the value

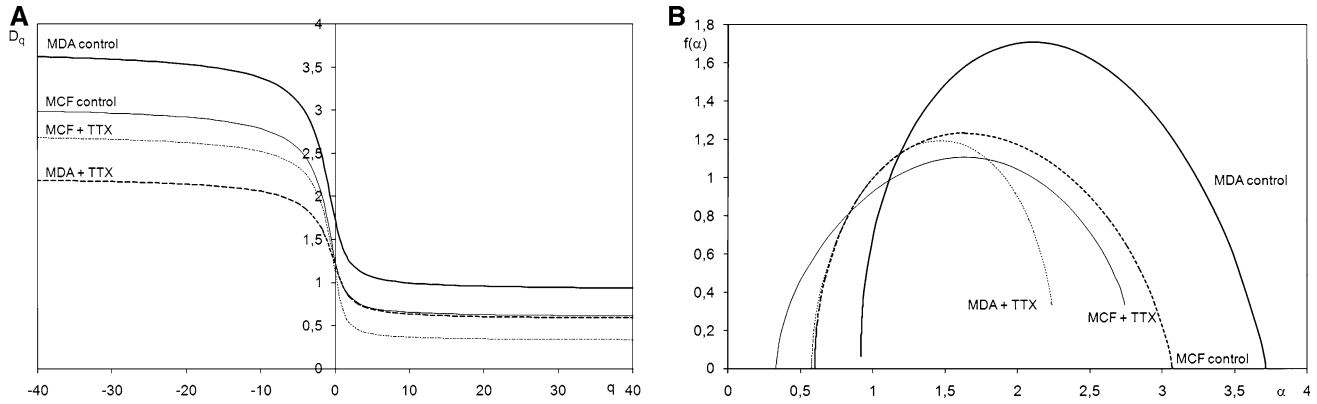

Fig. 5 Averaged profiles of the generalized fractal dimension D_q (**a**) and $f(\alpha)$ spectrum (**b**) for MDA-MB-231 (MDA) and MCF-7 (MCF) cells under control and TTX (1 μM) treated conditions. *Inset* in (**a**) applies to both parts

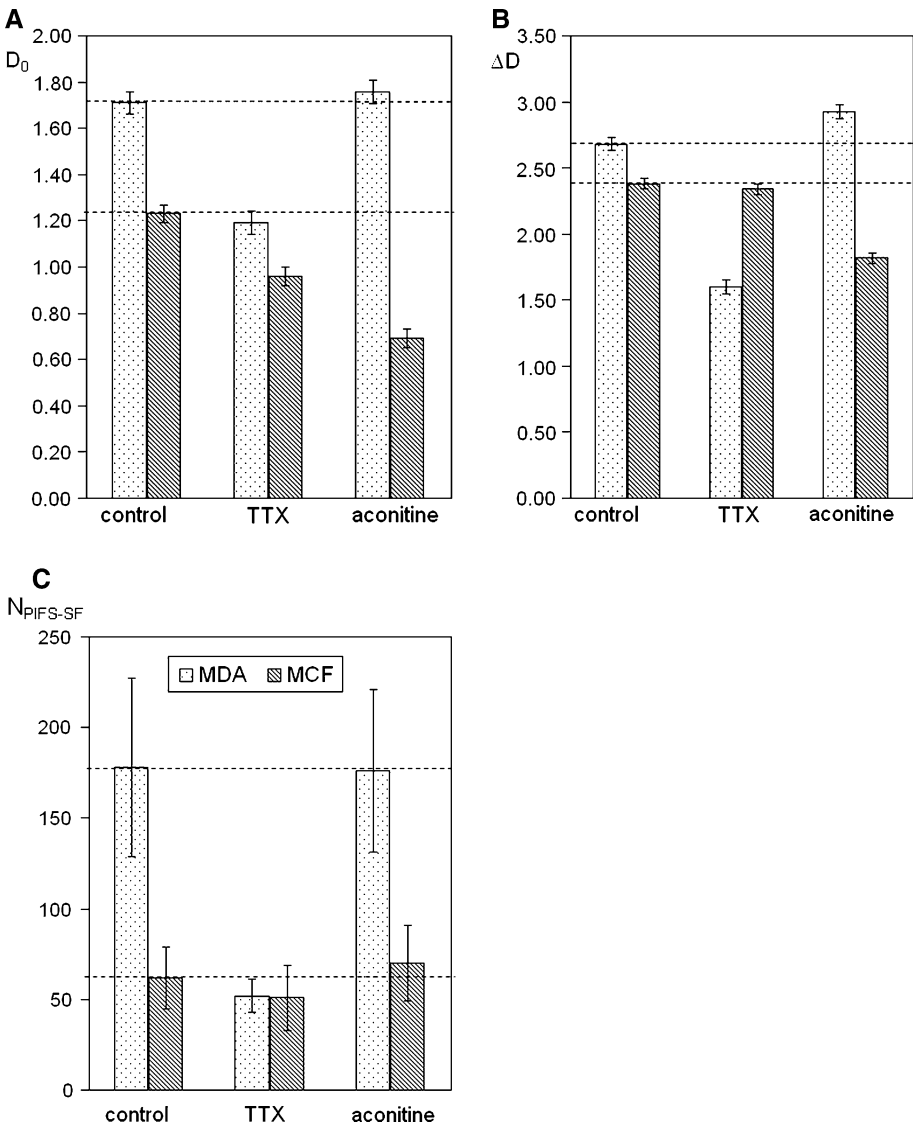

Fig. 6 Values of the fractal dimension D_0 (**a**), the parameter ΔD [width of $f(\alpha)$ spectrum, i.e., difference between D_∞ and $D_{-\infty}$] (**b**), and the number of PIFS-SF codes (**c**) determined for MDA-MB-231 and MCF-7 cells under control and 1 μM TTX pre-treated conditions. *Columns* denote the mean ± standard error. The *dotted horizontal lines* indicate the control levels for comparison

of ΔD (to 1.82 ± 0.05) but this was also not significant ($P > 0.05$).

Differences were also observed in the values of D_2, D_3, D_5, D_6, and D_{10} for MDA-MB-231 and MCF-7 cells under control conditions and following treatment with TTX (Table 2). However, these data have not been analyzed further due to the uncertainty of the physical meaning of these higher-order fractals. Finally, the analysis of $N_{PIFS\text{-}SF}S$ gave a clear result, and there was a significant difference in the values for MDA-MB-231 cells (178 ± 49) and MCF-7 cells (62 ± 17). TTX had an effect only on the former, with the value decreasing to 52 ± 9, whereupon the difference between the two cell lines disappeared ($P > 0.05$).

Discussion

The main results of the present study are as follows: (1) MDA-MB-231 cells were much more endocytic (and exocytic) than MCF-7 cells, in agreement with the former being strongly metastatic. (2) The quality of the vesicular activity (patterning) was also more complex for the MDA-MB-231 cells, with all main fractal parameters measured (D_0, ΔD, and $N_{PIFS\text{-}SF}S$) having greater values compared with MCF-7 cells. (3) The quantity and quality of vesicular activity in MDA-MB-231 cells were controlled (potentiated) by VGSC activity. There was no involvement of VGSC activity in MCF-7 cells. For almost every parameter measured, the difference between the two cell lines disappeared after VGSC activity was blocked with TTX. (4) Vesicular activity in MDA-MB-231 cells was strongly dependent on extracellular Na^+ but only partially dependent on Ca^{2+} (extracellular and intracellular) and PKA activity. As overall conclusions, we can state that (1) functional VGSC expression serves to enhance metastatic potential of cancer cells and (2) fractal methods are applicable to the study of vesicular activity in cancer cells (Krasowska et al. 2004a).

Technical aspects

We used HRP as a measure of endocytotic membrane activity. Previously, this method was used to determine endocytosis in two prostate cancer cell lines (Mycielska et al. 2003; Krasowska et al. 2004a). The parameter E quantified the amount of tracer uptake relative to cell size and revealed that the MDA-MB-231 cells were more endocytotic than MCF-7 cells, in line with the much stronger metastatic character of the former. Fractal dimension D_0 relates to the mass scaling of the object and can be complementary to E. Similar results were obtained previously for rodent PCa cell lines of different metastatic potential (Krasowska et al. 2004a).

VGSC involvement in cancer cell endocytic membrane activity

The metastatic MDA-MB-231 cells were shown previously to express functional VGSCs that were not found in the weakly nonmetastatic MCF-7 cells (Grimes and Djamgoz 1998; Diss et al. 2001; Roger et al. 2003; Fraser et al. 2005). Consistent with this, endocytic activity in MDA-MB-231 was shown to be highly sensitive to suppression of VGSC activity by TTX and extracellular Na^+ reduction (Fraser et al. 2005). Interestingly, aconitine (a VGSC "opener") caused a slight (but significant) increase in endocytic activity of MDA-MB-231 but not MCF-7 cells. These results suggested (1) that VGSC activity controlled endocytic activity in MDA-MB-2321 cells and (2) that this potentiating effect was near-maximal. Similar results were obtained previously from rat prostate cancer cells (Mycielska et al. 2003; Krasowska et al. 2004a).

At present, the nature of what is being trafficked and/or released by exocytosis (and reflected by endocytosis) under the influence of VGSC activity in BCa cells is not known, but some candidates can be considered. These include cathepsin (Roger et al. 2006), which is a well-known protease facilitating BCa cell invasiveness (Nomura and Katunuma 2005). The VGSC protein itself is also under activity-dependent internalization/externalization by positive feedback (Brackenbury et al. 2007). Finally, the possible role of VGSC activity in human PCa cell secretion was studied in a clinical context by testing the effects of anticonvulsant drugs. Thus, Abdul and Hoosein (2001) showed that secretion of prostate-specific antigen and IL-6 from human PCa cell lines was inhibited by phenytoin and carbamazepine (VGSC blockers).

Ionic control of vesicular activity in breast cancer cells

Endocytotic activity of MDA-MB-231 cells was completely dependent on extracellular Na^+, strongly dependent on intracellular Ca^{2+}, and partially dependent on PKA activity and extracellular Ca^{2+} (Fig. 4). The dependence on extracellular Na^+ (and lack of it in MCF-7 cells) is consistent with selective functional VGSC expression in the metastatic MDA-MB-231 cells (Fraser et al. 2005). As regards the mechanism(s) of control of endocytosis/exocytosis by VGSC activity (applicable to MDA-MB-231 cells), two general mechanisms can be considered: (1) Ca^{2+}-dependent. This is the "classic" mode in which VGSC-dependent depolarization opens voltage-gated Ca^{2+} channels (VGCCs) and allows in Ca^{2+} from extracellular medium. The subsequent rise in intracellular Ca^{2+} then

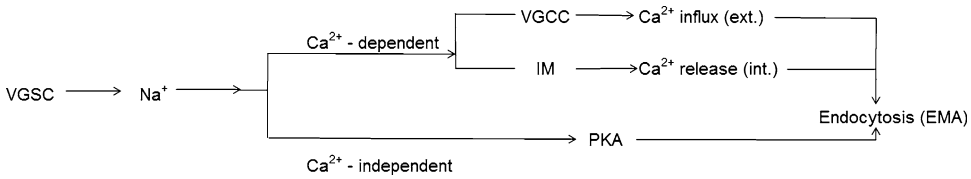

Fig. 7 Model for the Na^+ and Ca^{2+} dependence of endocytic membrane activity (EMA) in MDA-MB-231 cells

mobilizes vesicles. Involvement of such a plasma membrane channel (CaV3.2) was shown to control secretory activity in human neuroendocrine PCa cells (Gackiere et al. 2008). A rise in intracellular Ca^{2+} can also occur by release from an internal store (Doan et al. 1994) and/or reversal of Na^+–Ca^{2+} exchange (Torok 2007). Our results are consistent with both extracellular and intracellular pools of Ca^{2+} being involved in the endocytic activity. (2) Ca^{2+}-independent. In this mode, it is the activity of a kinase, frequently PKA, that mobilizes the vesicles (Kuromi and Kidokoro 2005). Indeed, inhibition of PKA reduced the amount of HRP uptake in MDA-MB-231 cells. Brackenbury and Djamgoz (2006) showed previously in rat PCa and Chioni et al. (2009) in MDA-MB-231 cells that Na^+ influx induced by VGSC activity can phosphorylate PKA.

From the data taken together, it is possible, therefore, that a model can be proposed for the Na^+ and Ca^{2+} dependence of endocytic membrane activity (EMA) in MDA-MB-231 cells (Fig. 7). In particular, this model is consistent with the total dependence on VGSC activity and extracellular Na^+, and the partial dependence on Ca^{2+} (extracellular and intracellular) and PKA activity. At present, we do not know why there is such a multiplicity of mechanisms controlling EMA in metastatic BCa cells. It is possible that the different mechanisms control the variety of endocytic activities in these cells, including the turnover of key signalling molecules (e.g., growth factor receptors, VGSC) and release of compounds, possibly with differing kinetics (Fig. 3).

Fractal analyses

Independent fractal analyses confirmed the results of the basic digital analyses and revealed that VGSC activity also controlled the patterning of vesicular uptake. Under control conditions, vesicles in MDA-MB-231 cells formed larger aggregates, irregularly distributed. Following the treatment with TTX, the vesicles became smaller and more dispersed, similar to the pattern seen in MCF-7 cells. Thus, endocytic membrane activity in BCa, which reflects the cells' metastatic potential, can be considered as a diffusive process and is amenable to fractal analyses.

The parameter D_0 ("fractal dimension") scales aggregation of mass with distance from the center and had a simple dependence on functional VGSC expression. Accordingly, the value of D_0 was higher for MDA-MB-231 than for MCF-7 cells, and the difference disappeared after treatment with TTX, which did not affect the latter. Thus, VGSC activity directly controlled the patterning of endocytic vesicles in MDA-MB-231 cells. The lack of an effect of aconitine (promoting VGSC activity) suggested that this control was fully developed under the basal conditions of the cells.

We used ΔD as a measure of "self-similarity" of sets, here, the degree of aggregation of vesicles within a cell. When an object is a stochastic fractal (with limited scale of self-similarity), the value of ΔD decreases with the increase in self-similarity. Under resting conditions, the value of ΔD was higher for MDA-MB-231 than for MCF-7 cells. Treating cells with TTX did not affect this parameter for MCF-7 cells, but in the case of the MDA-MB-231 cells, there was a significant decrease in the value of ΔD, which became lower than that of MCF-7 cells.

Differences were also observed in the values of D_2, D_3, D_5, D_6, and D_{10} for MDA-MB-231 and MCF-7 cells under control conditions and following treatment with TTX (Table 2). However, these data have not been analyzed further due to the uncertainty of the physical meaning of the fractals of higher order.

As can be seen from Table 2, $D_{|i|}$ ($i = 0, \pm1, \pm2,\ldots$) acquires significantly higher values for MDA-MB-231 than for MCF-7 cell line. $|i| \leq 2$ depicts the tendency to aggregate, whilst $|i| \geq -2$ the tendency to spread (see Fig. 1).

The $N_{PIFS\text{-}SF}$ value represents the "weight" of the staining, i.e., the larger the mass of staining and its spatial heterogeneity within the cell, the higher the value. Indeed, this parameter was also more developed for the metastatic cells and had a simple, direct dependence on VGSC activity.

Concluding remarks

In conclusion, multifractal analysis would appear overall to be highly suitable for quantitative analyses of the spatial organization of vesicles resulting from membrane endocytosis in human BCa cells. A similar conclusion was reached previously for strongly vs. weakly metastatic rat PCa cell lines (Krasowska et al. 2004a). The fact that the two cancers are similar is not surprising since they are both secretory epithelia and share a number of fundamental characteristics, including hormone sensitivity, functional VGSC expression, and metastatic targets, especially bone.

Thus, VGSC activity controls qualitative as well as quantitative aspects of vesicular activity in these cancer cells and can distinguish between strongly and weakly metastatic modes. Further studies are required to improve the understanding of the biophysical/physiological meaning of the fractal parameters and the precise mechanisms of their control by VGSC activity. This effort could benefit from extension of the approach to analyses of classic statistical aspects and lacunarity (Krasowska et al. 2004b; Borys et al. 2008). We have applied several fractal dimensions to describe and characterize vesicle distribution in breast and prostate cancer cells, and based on these studies, we can conclude that generalized fractal dimensions, particularly D_0, D_1, D_{-1}, and ΔD, can be potentially useful in cancer diagnostics. Further and more detailed studies are needed.

Based on the previous (Krasowska et al. 2004a) and present work we can conclude, therefore, that the vesicle patterns differ depending on the metastatic potential of cancer cells and can be characterized using fractal dimensions.

Acknowledgments This study was supported by the Pro Cancer Research Fund (PCRF), the Silesian University of Technology (grant BK221/RCH4/2006), and The British Council (Warsaw). Z.J.G. would like to acknowledge the warm and generous hospitality of Ealing Abbey during stays in London.

References

Abdul M, Hoosein N (2001) Inhibition by anticonvulsants of prostate-specific antigen and interleukin-6 secretion by human prostate cancer cells. Anticancer Res 31:2045–2048

Ali S, Coombes RC (2002) Endocrine-responsive breast cancer and strategies for combating resistance. Nat Rev Cancer 2:101–112

Almqvist N (1996) Fractal analysis of scanning probe microscopy images. Surf Sci 355:221–228

Anderson AR, Quaranta V (2008) Integrative mathematical oncology. Nat Rev Cancer 8:227–234

Avnir D (ed) (1989) The fractal approach to heterogeneous chemistry: surfaces, colloids, polymers. Wiley, New York

Baish WJ, Rakesh KJ (2000) Fractals and cancer. Cancer Res 60:3683–3688

Bassingthwaighte J, Liebovitch L, West B (1994) Fractal physiology. Oxford University Press, New York

Borys P, Krasowska M, Grzywna ZJ, Djamgoz MB, Mycielska ME (2008) Lacunarity as a novel measure of cancer cells behavior. Biosystems 94:276–281

Brackenbury WJ, Djamgoz MB (2006) Activity-dependent regulation of voltage-gated Na^+ channel expression in Mat-LyLu rat prostate cancer cell line. J Physiol 573:343–356

Brackenbury WJ, Chioni AM, Diss JKJ, Djamgoz MBA (2007) The neonatal splice variant of Nav1.5 potentiates in vitro invasive behaviour of MDA-MB-231 human breast cancer cells. Breast Cancer Res Treat 101:149–160

Chioni AM, Brackenbury WJ, Calhoun JD, Isom LL, Djamgoz MB (2009) A novel adhesion molecule in human breast cancer cells: voltage-gated Na(+) channel beta1 subunit. Int J Biochem Cell Biol 41:1216–1227

Coffey DS (1998) Self-organization, complexity and chaos: the new biology for medicine. Nat Med 4:882–885

Cross SS (1997) Fractals in pathology. J Pathol 182:1–8

Cross SS, Cotton DWK (1992) The fractal dimension may be a useful morphometric discriminant in histopathology. J Pathol 166:409–411

de Pillis LG, Radunskaya AE, Wiseman CL (2005) A validated mathematical model of cell-mediated immune response to tumor growth. Cancer Res 61:7950–7958

Diss JK, Archer SN, Hirano J, Fraser SP, Djamgoz MBA (2001) Expression profiles of voltage-gated Na^+ channel alpha-subunit genes in rat and human prostate cancer cell lines. Prostate 48:165–178

Djamgoz MBA, Krasowska M, Martinoli O, Sericano M, Vallerga S, Grzywna ZJ (2001) Structure-function correlation in transient amacrine cells of goldfish retina: basic and multifractal analyses of dendritic trees in distinct synaptic layers. J Neurosci Res 66:1208–1216

Doan TN, Gentry DL, Taylor AA, Elliott SJ (1994) Hydrogen peroxide activates agonist-sensitive Ca(2+)-flux pathways in canine venous endothelial cells. Biochem J 297:209–215

Eccles D, Gerty S, Simmonds P, Hammond V, Ennis S, Altman DG, POSH Steering Group (2007) Prospective study of outcomes in sporadic versus hereditary breast cancer (POSH): study protocol. BMC Cancer 7:160

Fong CW, Leong HF, Wong ES, Lim J, Yusoff P, Guy GR (2003) Tyrosine phosphorylation of Sprouty2 enhances its interaction with c-Cbl and is crucial for its function. J Biol Chem 278:33456–33464

Fraser SP, Diss JKJ, Chroni AM, Mycielska ME, Pan H, Yamach RF, Pani F, Siwy Z, Krasowska M, Grzywna ZJ, Backenbury WJ, Theodorom D, Koyuturk M, Kaya H, Battaloglu E, Tamburo de Bella M, Slade MJ, Tolhurdt R, Palmeri C, Jiang J, Lachman DS, Coombes RC, Djamgoz MB (2005) Voltage-gated sodium channel expression and potentiation of human breast cancer metastasis. Clin Cancer Res 11:5381–5389

Gackiere F, Bidaux G, Delcourt P, Van Coppenolle F, Katsoqiannou M, Drwailly E, Bavencoffe A, Van Chuoi-Mariot MT, Mauroy B, Prevarskaya N, Mariot P (2008) CaV3.2 T-type calcium channels are involved in calcium-dependent secretion of neuroendocrine prostate cancer cells. J Biol Chem 283:10162–10173

Grimes JA, Djamgoz MBA (1998) Electrophysiological characterization of voltage-gated Na^+ current expressed in the highly metastatic Mat-LyLu cell line of rat prostate cancer. J Cell Physiol 175:50–58

Grzywna ZJ, Stolarczyk J (2002) On some structure-morphology problems by the extended partitioned iterated function system (PIFS-SF). Chaos Solitons Fractals 13:897–905

Grzywna ZJ, Krasowska M, Ostrowski Ł, Stolarczyk J (2001) Can generalized dimension (D_q) and f(α) be used in structure-morphology analysis? Acta Phys Pol B 32:1561–1577

Grzywna ZJ, Krasowska M, Stolarczyk J (2003) On the application of PIFS-SF and D_q (f(α)) to dendrites analysis. Acta Phys Pol B 34:3681–3693

Gundelfinger ED, Kessels MM, Qualmann B (2003) Temporal and spatial coordination of exocytosis and endocytosis. Nat Rev Mol Cell Biol 4:127–139

Hall DJ, Martin DA, Kincaid K (2003) Filgrastim support during combination chemotherapy using cisplatin, doxorubicin, and cyclophosphamide to treat advanced or recurrent endometrial cancer: a clinical study and literature review. Eur J Gynaecol Oncol 24:481–489

Krasowska M, Grzywna ZJ, Mycielska ME, Djamgoz MB (2004a) Patterning of endocytotic vesicles and its control by voltage-gated Na^+ channel activity in rat prostate cancer cells: fractal analyses. Eur Biophys J 33:535–542

Krasowska M, Borys P, Grzywna ZJ (2004b) Lacunarity as a measure of texture. Acta Phys Pol B 35:1519–1534

Kuromi H, Kidokoro Y (2005) Exocytosis and endocytosis of synaptic vesicles and functional roles of vesicle pools: lessons from the Drosophila neuromuscular junction. Neuroscientist 11:138–147

Liang XJ, Mukherjee S, Shen DW, Maxfield FR, Gottesman MM (2006) Endocytic recycling compartments altered in cisplatin-resistant cancer cells. Cancer Res 66:2346–2353

Liebovitch LS (1998) Fractals and chaos simplified for the life sciences. Oxford University Press, New York

Liebovitch LS, Toth TI (1990) Using fractals to understand the opening and closing of ion channels. Ann Biomed Eng 18:177–194

Liotta LA (1986) Molecular biology of metastases: a review of recent approaches. Eur J Cancer Clin Oncol 22:345–348

Losa GA (1995) Fractals in pathology: are they really useful? Pathologica 87:310–317

Murakami Y, Tanaka J, Koshimura K, Kato Y (1998) Involvement of tetrodotoxin-sensitive sodium channels in rat growth hormone secretion induced by pituitary adenylate cyclase-activating polypeptide (PACAP). Regul Pept 73:119–121

Mycielska ME, Szatkowski M, Djamgoz MBA (2003) Contribution of functional voltage-gated Na^+ channel expression to cell behaviours in the matastatic cascade in rat prostate cancer. II. Secretory membrane activity. J Cell Physiol 195:461–469

Nomura T, Katunuma N (2005) Involvement of cathepsins in the invasion, metastasis and proliferation of cancer cells. J Med Invest 52:1–9

Oiwa NN, Glazier JA (2004) Self-similar mitochondrial DNA. Cell Biochem Biophys 41:41–62

Onganer PU, Djamgoz MBA (2005) Small-cell lung cancer (human): potentiation of endocytic membrane activity by voltage-gated Na^+ channel expression in vitro. J Membr Biol 204:67–75

Parkin DM, Pisani P, Ferlay J (1999) Estimates of the world-wide incidence of 25 major cancers in 1990. Int J Cancer 80:827–841

Polo S, Pece S, Di Fiore PP (2004) Endocytosis and cancer. Curr Opin Cell Biol 16:156–161

Roger S, Besson P, Le Guennec JY (2003) Involvement of a novel fast inward sodium current in the invasion capacity of a breast cancer cell line. Biochim Biophys Acta 1616:107–111

Roger S, Potier M, Vandier C, Besson P, Le Guennec JY (2006) Voltage-gated sodium channels: new targets in cancer therapy? Curr Pharm Des 12:3681–3695

Rubin J, Murphy TC, Zhu L, Roy E, Nanes MS, Fan X (2003) Mechanical strain differentially regulates endothelial nitric-oxide synthase and receptor activator of nuclear kappa B ligand expression via ERK1/2 MAPK. J Biol Chem 278:34018–34025

Schroeder M (1991) Fractals, chaos, power laws. W.H. Freeman, New York

Seino S, Shibasaki T (2005) PKA-dependent and PKA-independent pathways for cAMP-regulated exocytosis. Physiol Rev 85: 1303–1342

Simeonov R, Simeonova G (2006) Fractal dimension of canine mammary gland epithelial tumors on cytologic smears. Vet Clin Pathol 35:446–448

Stanley HG (1996) Fractals and multifractals: the interplay of physics and geometry. In: Bunde A, Havlin S (eds) Fractals and disordered systems. Springer, New York

Stosic T, Stosic BD (2006) Multifractal analysis of human retinal vessels. IEEE Trans Med Imaging 25:1101–1107

Torok TL (2007) Electrogenic Na^+/Ca^{2+}-exchange of nerve and muscle cells. Prog Neurobiol 82:287–347

Turiel A (2003) Relevance of multifractal textures in static images. Electr Letts Comp Vis Image Anal 1:35–49

Wong TW, Tracy E, Oseroff AR, Baumann H (2003) Photodynamic therapy mediates immediate loss of cellular responsiveness to cytokines and growth factors. Cancer Res 63:3812–3818